# A comparative study of human and porcine-derived decellularised nerve matrices

*Rui Li[1,2], Shuai Qiu[3], Weihong Yang[2,4], Zilong Rao[1], Jiaxin Chen[1], Yuexiong Yang[4], Qingtang Zhu[3,*], Xiaolin Liu[3], Ying Bai[1,*], Daping Quan[1,*]*

**Key Words:**
allogeneic; decellularised nerve matrix; immune response; xenogeneic; α-Gal

## From the Contents



## ABSTRACT

*Decellularised extracellular matrix (dECM) biomaterials originating from allogeneic and xenogeneic tissues have been broadly studied in the field of regenerative medicine and have already been used in clinical treatments. Allogeneic dECMs are considered more compatible, but they have the drawback of extremely limited human tissue sources. Their availability is also restricted by the health and age of the donors. To investigate the viability of xenogeneic tissues as a substitute for human tissues, we fabricated both porcine decellularised nerve matrix (pDNM) and human decellularised nerve matrix for a comprehensive comparison. Photomicrographs showed that both dECM scaffolds retained the ECM microstructures of native human nerve tissues. Proteomic analysis demonstrated that the protein compositions of both dECMs were also very similar to each other. Their functional ECM contents effectively promoted the proliferation, migration, and maturation of primary human Schwann cells in vitro. However, pDNM contained a few antigens that induced severe host immune responses in humanised mice. Interestingly, after removing the α-galactosidase antigen, the immune responses were highly alleviated and the pre-treated pDNM maintained a human decellularised nerve matrix-like pro-regenerative phenotype. Therefore, we believe that an α-galactosidase-free pDNM may serve as a viable substitute for human decellularised nerve matrix in future clinical applications.*

***Corresponding authors:**
Qingtang Zhu,
Zhuqingt@mail.sysu.edu.cn;
Ying Bai,
baiy28@mail.sysu.edu.cn;
Daping Quan,
cesqdp@mail.sysu.edu.cn.

http://doi.org/10.12336/biomatertransl.2023.03.006

**How to cite this article:**
Li, R.; Qiu, S.; Yang, W.; Rao, Z.; Chen, J.; Yang, Y.; Zhu, Q.; Liu, X.; Bai, Y.; Quan. D. A comparative study of human and porcine-derived decellularised nerve matrices. *Biomater Transl.* **2023**, *4*(3), 180-195.

## Introduction

The number of functional biomaterials composed of decellularised extracellular matrix (dECM) has been growing rapidly and they have drawn great attention regarding regenerative medicine.[1-3] Numerous applications of dECM scaffolds and hydrogels have been developed for peripheral nerve regeneration, musculoskeletal defect repair, wound healing, treatment of myocardial infarction, and therapeutic solutions for many other diseases.[4-6] dECM biomaterials, especially those derived from mammalian tissues, often exhibit specific bioactivity that is beneficial to facilitating cellular proliferation, migration, maturation, and directed differentiation, eventually promoting tissue remodelling.[7] It is worth noting that both xenogeneic and allogeneic tissues have been employed as original sources of biomaterials, which have been implanted in millions of patients for clinical treatments.[8-10]

Among many U.S. Food and Drug Administration-approved dECM scaffolds, those derived from allogeneic nerves provide off-the-shelf substitutes for nerve autografts (the gold standard) for functionally repairing peripheral nerve deficits.[11] Current commercialised decellularised nerve allografts, which include Avance (Axogen Inc., Alachua, FL, USA) and hANGs (Guangzhou Zhongda Medical Device Company, Guangzhou, China), maintain the nanofibrous structures and major components of the natural extracellular matrix (ECM) in human nerves.[11, 12] However, the practical use of such decellularised allografts is extremely limited by

the inadequate tissue supply as well as the great risk of disease transmission. Moreover, the allogeneic tissues are typically from old and cadaveric sources with large batch variability. The age of the source animal is one of the major factors that determines the biological function of dECM scaffolds. Those obtained from foetal/neonatal mammals result in greater regenerative performance than those produced from adult mammals.[13, 14]

Besides these commercialised decellularised nerve allografts, various xenogeneic dECM-based materials have been developed into functional scaffolds for peripheral nerve regeneration, as reported in many pre-clinical research studies.[9, 15, 16] Porcine decellularised nerve matrix (pDNM) has been processed in several other forms that allow customised fabrication of advanced nerve guidance conduits. For example, pDNM was intimately integrated into oriented electrospun nanofibres, which combined biological and topological nerve guidance and resulted in synergistic effects on directed neurite outgrowth and remyelination.[17-19] Additionally, pDNM can be further digested and form a hydrogel at ~37°C for easy processing or cell encapsulation. The pDNM pre-gel solution can be either directly injected into injury sites,[20] or perfused into pre-fabricated conduits for repairing peripheral nerve defects.[21, 22] Unlike clinical application of allogeneic dECM nerve grafts, the above-mentioned research studies used porcine dECM biomaterials and implanted them into xenogeneic animal models (mostly rodent sciatic nerve defect models), which demonstrated their beneficial properties in promoting nerve regeneration and functional recovery. Here we ask a question that is critical to biomaterials translation: can these xenogeneic dECM materials serve as viable substitutes for human decellularised nerve grafts for the clinical treatment of nerve defects? As a matter of fact, decellularised porcine tissues have been successfully commercialised and implanted into patients as biological scaffold materials, including dermis, heart valves, small intestinal submucosa, and others.[23] They are readily available and usually harvested from younger tissue sources.

Although both raw material sources have been used clinically, few comparative studies between the xenogeneic and allogeneic decellularised materials have been performed, and especially the host response to both materials is poorly understood. Although some research studies reported that dECM may suppress inflammatory responses after xenogeneic graft implantation into non-human animal models,[24, 25] a few cell surface antigens found in the tissue-derived dECM materials can potentially provoke host rejection or other immunogenic responses. For example, the galactosidase (Gal) epitope is commonly present in non-primate mammalian tissue but not in primates.[26] Compared to the innate immune response, very few studies have investigated changes in the acquired immune system following dECM scaffold implantation. Animal studies are typically used for biocompatibility assessments, but the immune cell receptors are distinctly different from those in humans.[27] On the other hand, considering the difficulties with conducting clinical trials or obtaining patient biopsies, the human immune response to these implanted biomaterials is hard to predict.

Herein, a comparative study was conducted to provide a comprehensive understanding of human and porcine decellularised nerve matrices (hDNM and pDNM), with respect to their microstructures, compositions, bioactivities, and the human immune responses post-implantation. First, the microstructures of both hDNM and pDNM were observed by scanning electron microscopy (SEM) and compared with each other after optimised decellularisation. Second, proteomic analysis revealed the compositional similarities and differences between the two materials. To briefly examine the bioavailability of both dECM materials, primary human Schwann cells (HSCs) were cultured on hydrogels derived from hDNM (hDNM-gel) and pDNM (pDNM-gel) for *in vitro* characterisation and comparison. Finally, the host response to the xenogeneic pDNM and allogeneic hDNM was assessed using a humanised mouse model. Hopefully, this comparative study can provide some insights into the clinical translations of tissue-derived dECM materials, especially pDNM which may serve as a substitute for decellularised hDNM allografts for the restoration of peripheral nerve defects.

## Methods

### Preparation of hDNM and pDNM

Human peripheral nerves (sciatic nerve) were obtained from Guangzhou Zhongda Medical Equipment Co., Ltd. (Guangzhou, China), and the study was approved by National Medical Products Administration of China (approval No. 20163131598, approved on August 26, 2021). Preparation of hDNM was performed according to a protocol described previously.[12] Briefly, the nerves were washed and then soaked in phosphate-buffered saline (PBS; B040100, Sangon Biotech, Shanghai, China) overnight. Then, the nerve tissues were agitated and rinsed in deionised water three times for 2 hours each time. The washed nerves were transferred to 3.0% (w/v) Triton X-100 (X100PC, Sigma-Aldrich, St. Louis, MO, USA) in PBS for 12 hours, and subsequently immersed in 4.0% sodium deoxycholate-containing PBS for another 6 hours. The resulting decellularised nerves were rinsed with deionised water for 1 day, followed by washing in isopropyl alcohol for 12 hours to remove lipids. Finally, after freezing at –40°C for 4 hours, the decellularised tissues were lyophilised for 2 days to produce the hDNM scaffolds.

The pDNM scaffolds were prepared by following a previously-reported protocol.[21] Briefly, the raw middle part of sciatic nerves and the corresponding distal end were harvested from miniature pigs (provided by the Experimental Animal Centre

1 Guangdong Engineering Technology Research Centre for Functional Biomaterials, School of Materials Science and Engineering, Sun Yat-sen University, Guangzhou, Guangdong Province, China; 2 Key Laboratory for Polymeric Composite & Functional Materials of Ministry of Education, School of Chemistry, Sun Yat-sen University, Guangzhou, Guangdong Province, China; 3 Guangdong Engineering Technology Research Centre for Peripheral Nerve Tissue, Department of Orthopaedic and Microsurgery, The First Affiliated Hospital of Sun Yat-sen University, Guangzhou, Guangdong Province, China; 4 Guangzhou Zhongda Medical Equipment Co., Ltd., Guangzhou, Guangdong Province, China

of the First Affiliated Hospital of Sun Yat-sen University), then decellularised by sequential treatment with 3.0% Triton X-100, 4.0% sodium deoxycholate, and rinsed with sterile water. Finally, the pDNM scaffold was obtained after degreasing with a mixed solvent (ethanol:dichloromethane = 1:2) and lyophilisation.

### Scanning electron microscopy

The microstructures of both hDNM and pDNM were characterised by SEM (JSM-6380LA, Jeol Ltd., Tokyo, Japan). The sample preparation was implemented using a previously-reported method.[28] Briefly, both hDNM and pDNM scaffolds were cut into small pieces and mounted on aluminium sample stubs. Their cross-sections were sputtered with platinum/palladium and then subjected to observation using an SEM.

### Histological staining

The hDNM and pDNM scaffolds were fixed in 4% paraformaldehyde (P0099, Beyotime Biotechnology, Shanghai, China) at 4°C for 12 hours. The fixed samples were dehydrated in graded alcohol, embedded in paraffin, and sectioned into 5-μm pieces. The sections were deparaffinised and then stained with haematoxylin-eosin by following the manufacturer's protocols (C0105, Beyotime Biotechnology). All samples were observed and images captured under a microscope (Leica Microsystems, Wetzlar, Germany).

### Residual DNA detection

Samples of hDNM and pDNM (5 mg each) were digested in proteinase K solution (200 μL, 1 mg/mL; ST533, Beyotime Biotechnology) at 56°C until digestion was complete. After centrifugation at 10,190 × *g* for 10 minutes, the DNA content of the supernatant was determined using a Quant-iT PicoGreen kit (P11496, Invitrogen, Carlsbad, CA, USA) according to the YY/T 0606.25-2014 standard.[21]

### Liquid chromatography-tandem mass spectrometry

Proteomic analysis of both hDNM and pDNM was performed by liquid chromatography-tandem mass spectrometry (LC-MS/MS).[29] Each dECM sample was added to sodium dodecyl sulphate lysis buffer (P0013G, Beyotime Biotechnology) at sample: buffer = 1:100 and then centrifuged at 14,000 × g for 30 minutes. The supernatant was analysed using a bicinchoninic acid protein assay kit (P0009, Beyotime Biotechnology). Afterwards, the proteins within the supernatant were digested with 25 μL trypsin solution, vortexed, and then incubated at 37°C overnight. The digested peptides were then desalted using Pierce C18 spin tips (90011, Thermo Fisher Scientific, Waltham, MA, USA). Peptide separation was implemented using high pH reverse-phase high-performance liquid chromatography on a C18 column. Finally, the isolated peptides were resuspended in 30 μL of solvent mixture (0.1% formic acid in acetonitrile) and analysed by online nanospray LC-MS/MS on an Orbitrap Fusion coupled to an EASY-nano-LC system (EASY-Nlc, Thermo Fisher Scientific).

### Proteomic analysis

The raw data from the mass spectrometer were analysed using Protein Discoverer 2.1 (Thermo Fisher Scientific) against the porcine and mammalian protein UniProt database (https://www.uniprot.org/help/publications).[30] All searches required 10 ppm precursor mass tolerance, 0.02 Da fragment mass tolerance, strict tryptic cleavage up to two missed cleavages, and 1% protein false discovery rate.[31] Using these conditions, the protein expression values were obtained and corrected using $\log_2$ transformation. Meanwhile, the mean value of each protein in the pDNM and hDNM samples was calculated, termed pDNM and hDNM, respectively. The ratio of pDNM to hDNM was defended as the FoldChange. To identify differentially-expressed proteins, the value of $\log_2$FoldChange > 1 with adjusted *P*-value < 0.05 was used to identify those which were up-regulated, while the value of $\log_2$FoldChange < −1 with adjusted *P*-value < 0.05 was used to identify down-regulated proteins. Matrisome annotations of both porcine and human nerves were identified and classified using MatrisomeDB 2.0 (http://www.matrisomedb.org).[32] The proteomics figures, including unsupervised hierarchical clustering images, were generated using the DESeq package in the R language software (version 3.2.3, https://www.r-project.org/).

### Preparation of hDNM-gel and pDNM-gel

To obtain the hDNM-gel and pDNM-gel, the lyophilised hDNM and pDNM scaffolds were first ground into powder using a Thomas Model 4 Wiley® Mill (Thomas Scientific, MA, USA). Then, the hDNM and pDNM powders were digested in 1 mg/mL pepsin dissolved in 0.01 M HCl (C0680110213, Nanjing Reagent, Nanjing, China). The digested solution was subjected to centrifugation at 44,760 × *g* (Optima MAX-XP, Beckman Coulter, Brea, CA, USA) for 30 minutes to remove all the undissolved particulates. Afterwards, the solution was neutralised to pH ~7.4 using 0.1 M NaOH (BD27, Guangzhou Chemical reagent Factory, Guangzhou, China) and diluted to reach an ionic equilibrium using 10× PBS (P1022-500, Solarbio, Beijing, China). The pre-gel solution was stored at −20°C or gelled at 37°C to obtain either hDNM-gel or pDNM-gel. The final concentration of both hydrogels was 1% (w/v).

### Preparation of primary human Schwann cells

HSCs (Cat# 1700, ScienCell Research Laboratories, San Diego, CA, USA) were isolated from human spinal nerves. They were cultured in Schwann cell medium (P60123, ScienCell Research Laboratories) containing 1% Schwann cell growth supplement, 1% penicillin/streptomycin, and 10% foetal bovine serum. The HSCs were incubated at 37°C in a humidified 5% $CO_2$ incubator. After two passages, 1 × $10^6$ cells per well were seeded into 6-well plates pre-coated with 0.5% (w/v) hDNM-gel or pDNM-gel, respectively.

### Viability test

HSCs were seeded into 6-well plates pre-coated with hDNM-gel or pDNM-gel, as appropriate. After 2 days of culture, the medium was replaced with PBS containing live/dead staining reagent (1 mM) and incubated in the dark for 30 minutes, then images of the cells were captured for counting using a fluorescence microscope (Nikon, Tokyo, Japan).

### Proliferation assessment

HSC proliferation was evaluated through 5-ethynyl-2′-deoxyuridine (EdU) labelling. After 24-hour incubation, the Schwann cell culture medium in each well was replaced with 200 μL fresh medium supplemented with EdU (final concentration 1 μM; C10310-3, RiboBio, Guangzhou, China). HSCs were then cultured for another 24 hours and fixed in 4% paraformaldehyde for 30 minutes. DNA incorporating EdU was labelled using an Alexa Fluor 488 Click-iT assay kit by following the manufacturer's instructions. Briefly, 1× Apollo dye reaction solution (100 μL) in combination with primary S100 antibody (mouse monoclonal, 1:1000, Cat# ab4066, Abcam, Cambridge, UK) was added to each well. After incubating for 2 hours at 37°C, cells were incubated with the goat anti-rabbit IgG Alexa Fluor 594-conjugated secondary antibody (1:5000, ab150080, Abcam) for 1 hour at 37°C. Next, cells were rinsed with PBS for 0.5 hour and their nuclei were stained with 6-diamidino-2-phenylindole-dihydrochloride (1 mM, C1006, Beyotime Biotechnology) in PBS for 10 minutes. Finally, observations were performed using a confocal microscope (LSM 900, Carl Zeiss Microscopy GmbH, Jena, Germany). The number of $EdU^+$ cells was quantified in at least three randomly-selected fields per sample ($n = 4$).

### Cell migration

HSC migration was assessed by a wound-healing scratch assay. Cells were seeded into 6-well plates pre-coated with either hDNM-gel or pDNM-gel, and cultured until confluence. Then, a sterile 200 μL pipette tip was used to create a uniform linear scratch across the centre of the wells. Each well was rinsed with medium to remove the detached cells, and the remaining cells were incubated under standard culture conditions for another 24 hours. Images of cell migration across the wound were acquired immediately after scratching and after culture for 24 hours using a fluorescence microscope (Nikon). The migration rate was measured using ImageJ software (V1.8.0.112, National Institutes of Health, Bethesda, MD, USA).[33] Migration rate was calculated as follows:

$$Migration\ rate\ (\%) = \left(\frac{D_0 - D_t}{D_0}\right) \times 100\% \quad (1)$$

where $D_0$ and $D_t$ represent the gap distance immediately after scratching and the width of the wound after 24 hours, respectively.

### Quantitative polymerase chain reaction

HSCs cultured on hDNM-gel/pDNM-gel were harvested on day 2. Total RNA was extracted from the cultured cells using TRIzol reagent (15596-018, Invitrogen), following the manufacturer's instructions. Equal amounts of total RNA were subjected to reverse transcription using a Prime Script™ RT reagent kit (RR047Q, TaKaRa, Kyoto, Japan). Quantitative polymerase chain reaction (qPCR) amplification was performed on an Applied Biosystems Step One Real-Time PCR System using a SYBR Premix Ex Taq™ Kit (RR820A, Takara). Relative fold changes in mRNA expression were calculated using the formula $2^{-\Delta\Delta Ct}$ method.[34] The fluorescence threshold (Ct) values were obtained from the SDS Enterprise Database software (Sphera). The primer sequences used in this study are shown in **Table 1**.

**Table 1. Primer sequences used for quantitative polymerase chain reaction**

| Gene | Primer sequence | Product size (bp) |
|---|---|---|
| MAP-2 | Forward: 5'-CTT CAC GCA CAC CAG GCA CTC-3' | 102 |
| | Reverse: 5'-CCT TCT TCT CAC TCG GCA CCA AG-3' | |
| GAP43 | Forward: 5'-TCC ACT GAT AAC TCG CCG TCC TC-3' | 94 |
| | Reverse: 5'-CAG CAG CAG TGA CAG CAG CAG-3' | |
| MBP | Forward: 5'-CGA GGA CGG AGA TGA GGA GTA GTC-3' | 197 |
| | Reverse: 5'-CAG CTC AGC GAC GCA GAG TG-3' | |
| MPZ | Forward: 5'-TGG TGC TGT TGC TGC TGC TG-3' | 185 |
| | Reverse: 5'-GGT GCT TCT GCT GTG GTC CAG-3' | |
| GFAP | Forward: 5'-GCT GCG GCT CGA TCA ACT CAC-3' | 169 |
| | Reverse: 5'-GGT GGC TTC ATC TGC TTC CTG TC-3' | |
| S100β | Forward: 5'-ACA ATG ATG GAG ACG GCG AAT GTG-3' | 80 |
| | Reverse: 5'-GAA CTC GTG GCA GGC AGT AGT AAC-3' | |
| β-Actin | Forward: 5'-GCA AGT GCT TCT AGG CGG ACT G-3' | 195 |
| | Reverse: 5'-CTG CTG TCA CCT TCA CCG TTC C-3' | |

Note: ECM: extracellular matrix; GAP43: growth-associated protein 43; GFAP: glial fibrillary acidic protein; MAP-2: microtubule-associated protein-2; MBP: myelin basic protein; MPZ: myelin protein zero.

### Preparation of pDNM-enzymolysis

To eliminate the α-Gal antigen in the pDNM, pDNM-enzymolysis was prepared according to a previously-described method with a slight modification.[35] Briefly, the lyophilised pDNM samples were incubated with 100 U/mL α-galactosidase (G8507, Merck, Darmstadt, Germany) for 4 hours at 25°C with gentle agitation. Then, the samples were washed with PBS solution three times, 30 minutes each time, followed by immersion in saline overnight to completely remove the residual enzyme.

### Detection of α-Gal antigen

The content of the α-Gal antigen was characterised using western blotting, immunofluorescence staining, and enzyme-linked immunosorbent assay.

#### *Western blot*

The hDNM, pDNM, and pDNM-enzymolysis samples were lysed by RIPA buffer (P0013, Beyotime Biotechnology). After quantification by bicinchoninic acid assay, the obtained proteins were separated and transferred to polyvinylidene fluoride membranes (IPVH00010, Millipore, Bedford, MA, USA). Afterwards, the membranes were treated with primary α-Gal antibody (human polyclonal, 1:1000, Santa Cruz Biotechnology, Santa Cruz, CA, USA, Cat# sc-517442) overnight, followed by horseradish peroxidase-conjugated secondary antibody (anti-rabbit, 1:10,000, Bioworld, Nanjing, China, Cat# BS13278) at 37°C for 1 hour. Finally, the membranes were assessed using a chemiluminescence ECL kit (P0018FS, Beyotime Biotechnology) and the results were observed using the ChemiDoc™ XRS+ Imaging System (GelDoc XR+, Bio-Rad, Hercules, CA, USA). Western blotting of MHC-1 in both hDNM and pDNM scaffolds followed a similar procedure except that a primary MHC-1 antibody (human polyclonal, 1:1000, Abcam, Cat# ab134189) was used.

#### *Immunofluorescence staining*

The samples were cut into 10-μm-thick sections and washed three times with 0.01 M PBS. After blocking with 5% bovine serum albumin (HY-D0842, MedChemExpress, Newark, NJ, USA) for 30 minutes, the specimens were incubated with primary α-Gal antibody (1:1000) overnight at 4°C. Then a rabbit anti-human IgG Alexa Fluor 488-conjugated secondary antibody (1:5000, Abcam, Cat# ab150189) was added and the samples were incubated at 37°C for 1 hour. Immunofluorescence images were obtained using a confocal laser microscope (DM6000, Leica Microsystems). The mean grey value of α-Gal was calculated using the integrated density divided by the area of the selected region. These parameters were quantified using ImageJ software. Images of five randomly-selected fields in each sample and three samples in each group were subjected to statistical analysis.

#### *Enzyme-linked immunosorbent assay*

The dissected nerve tissues with/without decellularisation and the pDNM-enzymolysis samples were weighed and mixed in radio immunoprecipitation assay lysis buffer. After centrifugation at 1790 × *g* for 10 minutes, the α-Gal in the supernatants was quantified using an α-Gal Antigen Quantitative Detection Kit (7010, SanYao Science & Technology Co, Beijing, China) according to the manufacturer's instructions. Briefly, after premixing with the dilution buffer, the samples were incubated in 96-well microplates coated with α-Gal antibody for incubation at room temperature for 1 hour. Then, 200 μL volume of α-Gal antibody working solution was added to each well and incubated at room temperature for another 2 hours. Subsequently, the tetramethylbenzidine substrate solution (100 μL/well) was added to enable the reaction at 25°C for 30 minutes. The reaction was stopped by adding stop solution (50 μL/well). The enzyme-linked immunosorbent assay results were obtained at 450 nm with a microplate reader (Thermo Fisher Scientific, MA, USA).

### Detection of endotoxin

Chromogenic endpoint *Tachypleus amebocyte* lysate (Chinese Horseshoe Crab Reagent Manufactory, Xiamen, China) was used for endotoxin quantification, which was carried out according to the manufacturer's protocol. Briefly, pDNM or hDNM suspension (10 mg/mL, 100 μL) plus Tachypleus amebocyte lysate (100 μL) were sequentially added to a 96-well plate. After incubating at 37°C for 10 minutes, 100 μL chromogenic matrix solution was added to each well. After 15 minutes, 500 μL azo reagent solution was added to each well. The absorbance of each well was measured with a microplate reader (545 nm, Thermo Fisher Scientific). This experiment was repeated three times. The linearity of the standard was verified using endotoxin standard solution.

### Humanised mouse model

The female mice (20–25 g) used for immune evaluation were peripheral blood mononuclear cell-NOD-Prkdcscid Il2rg$^{null}$ (PBMC-NPG) mice (Stock No. VS-AM-004, also termed Hu-mice), which were purchased from Beijing Vitalstar Biotechnology, aged 8–10 weeks. All animal experiments were performed in accordance with a protocol that was approved by the Institutional Animal Care and Use Committee of Beijing Vitalstar Biotechnology Company (approval No. VST-SY-20191008, approval date: October 8, 2019), and were designed and reported according to the Animal Research: Reporting of *In Vivo* Experiments (ARRIVE) guidelines.[36] NPG immunodeficient mice were conditioned with sublethal (1.4 Gy) whole-body irradiation.[37] After 6 hours of irradiation, the animals were transfused intravenously with $2 \times 10^7$ human peripheral blood mononuclear cells (PBMCs) isolated from the peripheral blood of healthy adult donors.[38] Then, the mice were employed for dECM immunity experiments for 8 weeks.

### Immune response *in vivo* assay

To evaluate the host immune response in humanised mice, the pDNM or hDNM solutions were injected into PBMC-NPG mice subcutaneously. Biomaterial injection and harvesting were performed following a previously-reported approach (**Additional Figure 1**).[39] After anaesthesia with 1.8% isoflurane (Forene™, Abbott Laboratories SA, IL, USA) in $O_2/N_2$ (30%/70%) for 5 minutes, each animal was pre-injected with 100 μL of sterile black ink in the back to visually label the matrices for ease of identification upon harvesting. Subsequently, four sites of the same dorsal region received a single type of dECM solution (pDNM or hDNM, 10 mg/mL, 250 μL per site) by evenly spaced subcutaneous injections. One week post injection, the animals were deeply anaesthetised by inhaling 1.8% isoflurane and transcardially perfused with 10 mL 0.9% normal saline, followed by 10 mL of ice-cold 4% paraformaldehyde in 0.1 M PBS. The subcutaneous tissue with all the injection sites, together with their neighbouring regions, was harvested for histological analysis.

Furthermore, the adaptive immune responses of both dECMs were examined using the same humanised mouse model. The PBMC-NPG mice were injected with 1 mL pDNM, hDNM, or pDNM-enzymolysis solution (concentration = 10 mg/mL) through the caudal vein during isoflurane anaesthesia. One week after injection, the venous blood was harvested from the eyeballs and collected into heparin anticoagulant tubes for flow cytometry.

In the above-mentioned two processes, each experiment contained four groups ($n$ = 3 for each group): control, hDNM, pDNM, and pDNM-enzymolysis groups. The PBMC-NPG mice that received 1 mL pDNM, hDNM, or pDNM-enzymolysis solution were regarded as hDNM, pDNM, and pDNM-enzymolysis groups, respectively. The control group received the same volume of sterile normal saline.

### Flow cytometry

The blood cells collected in heparin anticoagulant tubes were washed with PBS and incubated with the antibody panel for 30–45 minutes at 4°C in the dark. Then, the cells were lysed with Pharm Lyse (Cat# 555899, BD Biosciences, San Jose, CA, USA) for 4 minutes. After centrifugation, the samples were suspended in PBS for data acquisition by flow cytometry (BD FACSCanto II, Beckman Coulter). Fluorochrome-conjugated monoclonal antibodies to the following human or mouse antigens were used: FITC-anti mouse CD45 (Biolegend, San Diego, CA, USA, Cat# 147710, RRID: AB_2563541), PE-anti human CD45 (Biolegend, Cat# 304039, RRID: AB_314395), FITC-anti human CD45 (Biolegend, Cat# 304038, RRID: AB_314393), PE-anti human CD3 (Biolegend, Cat# 300308, RRID: AB_314043), APC-anti human CD19 (Biolegend, Cat# 392506, RRID:AB_2750096), PE-Cy7 anti human CD4 (Biolegend, Cat# 357410, RRID: AB_2565661), APC-anti human CD8 (Biolegend, Cat# 344722, RRID: AB_2075390). A FACSCalibur instrument and Cellquest software were used for flow cytometry analysis.

### Statistical analysis

Pearson's correlation analysis was performed using IBM SPSS Statistics 27 (Armonk, NY, USA). The other statistical analyses were performed using GraphPad Prism 8.0.2 (GraphPad Software Inc., La Jolla, CA, USA, www.graphpad.com). The data are expressed as mean ± standard deviation (SD) for continuous variables. When three groups of data were compared, one-way analysis of variance followed by Tukey's *post hoc* test was used. Differences were considered statistically significant when $P < 0.05$.

## Results

### Decellularisation and structural characterisations of hDNM and pDNM

The cross-sectional morphologies of the native nerve tissues in both human and porcine showed substantial nerve tract-like ellipsoidal shape (**Additional Figure 2**). After optimised decellularisation, the ultrastructures of hDNM and pDNM were characterised by SEM (**Figure 1A–D**). As shown in **Figure 1A1** and **B1**, both DNM scaffolds were composed of many decellularised nerve bundles/fascicles and interfascicular connective tissues. Higher resolution micrographs showed that each nerve fascicle consisted of numerous microchannels with diameters ranging from 5 to 20 μm (**Figure 1A2–4** and **B2–4**). Furthermore, the longitudinal view of both DNM scaffolds showed lamellar microstructures with rather smooth surfaces (**Figure 1C1** and **D1**). The magnified images clearly showed that these laminar structures (i.e., endoneurium) were formed by closely-assembled and longitudinally-aligned nanofibres, each with a diameter of ~100 nm (**Figure 1C2**, **3** and **D2**, **3**). It was apparent that both hDNM and pDNM consisted of similar micro- and nanostructures, and no significant differences were found between the two scaffolds, except for the slightly misaligned nanofibres found in hDNM (**Figure 1C3**) and the randomly-distributed microbeads on the pDNM. These minor variations were most likely due to the slight disparities in decellularisation protocols.

Results from haematoxylin-eosin staining showed that cellular content in either dECM scaffold, implying that both nerve tissues underwent complete decellularisation (**Figure 1E**). In the hDNM, the shape of nerve tracts was almost intact after decellularisation, while the pDNM revealed a slightly disordered extracellular matrix of the porcine sciatic nerves. Moreover, DNA content in the dECM scaffolds was also quantified (**Figure 1F**). The result showed that the DNA content in native human nerves and native porcine nerves was 572.6 ± 161.2 ng/mg and 300.9 ± 116.9 ng/mg, respectively. After decellularisation, their DNA contents were reduced approximately 94.1% (native human nerve) and 88.1% (native porcine nerve). Nevertheless, enzyme digestion did not further reduce the content of residual DNA (hDNM *vs.* hDNM-gel: $P > 0.05$; hDNM *vs.* hDNM-gel: $P > 0.05$). The minimal residual DNA content in hDNM (34.2 ± 9.5 ng/mg), hDNM-gel (33.3 ± 7.7 ng/mg), pDNM (36.1 ± 11.2 ng/mg) and pDNM-gel (28.8 ± 11.8 ng/mg) met the globally-recognised standard (50 ng/mg).[40] Although repeated and intensive chemical decellularisation would further reduce the residual DNA content within the hDNM and pDNM, their composition and microstructures might also be seriously damaged under such harsh conditions.

### Proteomic analysis of hDNM and pDNM

Since the dECMs consist of numerous types of proteins from the native nerve tissues, the compositions of pDNM and hDNM were identified by LC-MS/MS and compared by proteomic analysis. After Pearson's correlation analysis, it was noticed that the unsupervised hierarchical clustering in the pDNM and hDNM samples were highly correlated with each other, but clustered separately between different groups (**Figure 2A**). Through mass spectrometric analysis, it was noted that the pDNM and hDNM shared 1431 characterised proteins in common, while 46 proteins in pDNM were upregulated and 48 proteins were downregulated compared to hDNM (**Figure 2B**). The protein compositions in each dECM sample are shown as a heatmap (**Figure 2C**). The proteomics results confirmed that the major components of pDNM and hDNM have the same functionalities, except for the minor protein species that are more specific corresponding to their original tissue sources.

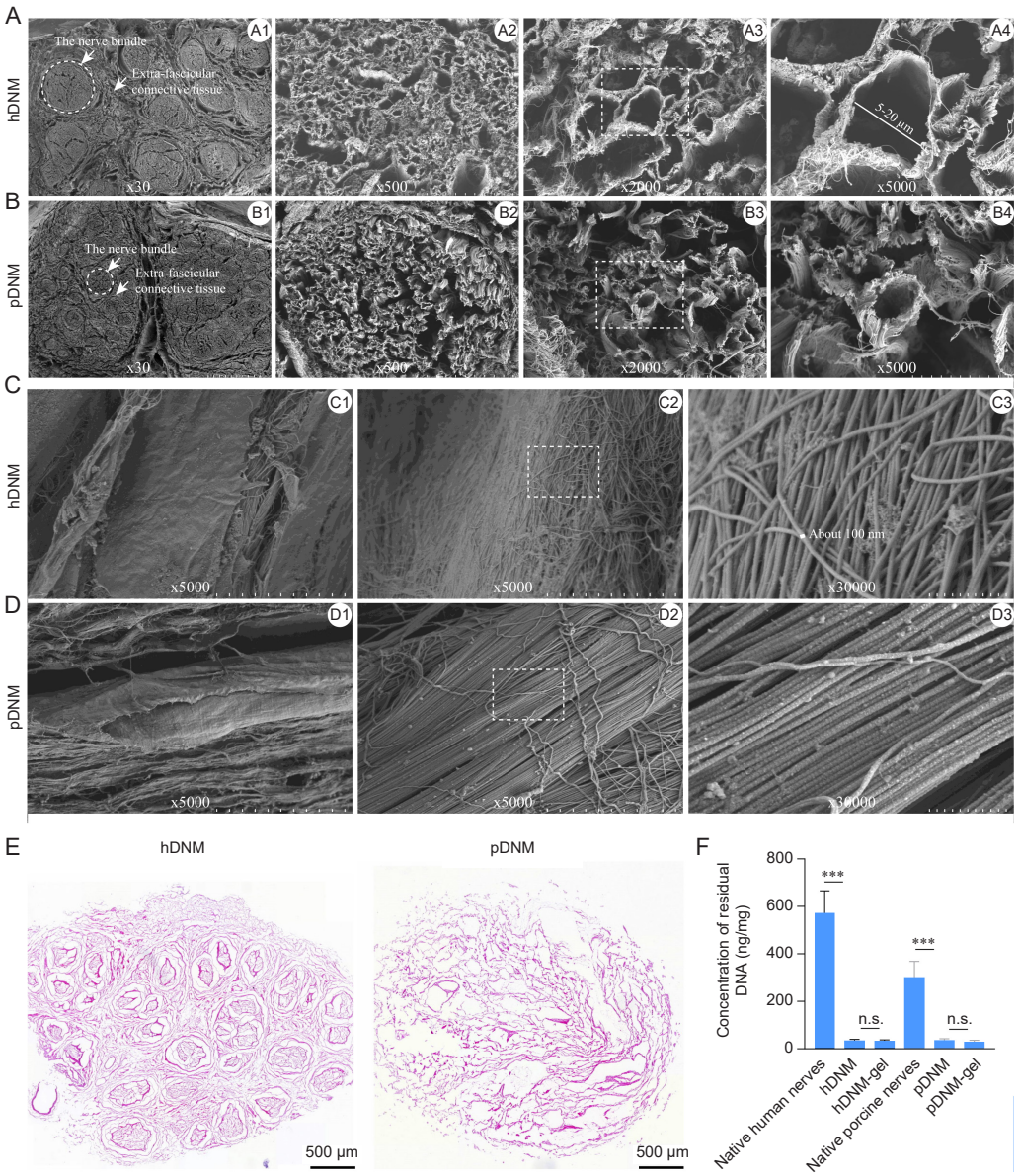


**Figure 1.** Structural and histological characterisations of the hDNM and pDNM scaffolds. Representative SEM micrographs of the hDNM (A) and pDNM (B) at lower magnification. Representative SEM micrographs of the hDNM (C) and pDNM (D) at higher magnification. Scale bars: 1 mm in A1, B1; 100 μm in A2, B2; 20 μm in A3, B3; 10 μm in A4, B4, C1, C2, D1, D2; and 1 μm in C3, D3. (E) Representative micrographs of hDNM and pDNM cross-sections after H&E staining. Scale bars: 500 μm. (F) DNA content quantified in the fresh tissues, hDNM, pDNM, hDNM-gel and pDNM-gel. Data are expressed as mean ± SD ($n$ = 4). ***$P$ < 0.001. H&E: haematoxylin-eosin; hDNM: human decellularised nerve matrix; n.s: not significant; pDNM: porcine decellularised nerve matrix; SEM: scanning electron microscopy.

We further investigated the diversity of ECM proteins identified in the hDNM and pDNM using an ECM-specific categorisation database, Matrisome DB 2.0. The ECM proteins, which are often divided into two categories: core matrisome and matrisome-associated proteins, are essential for tissue morphogenesis, differentiation, and homeostasis. As shown in the Venn diagram (**Figure 3A**), 68 ECM proteins were identified in the pDNM samples. Meanwhile, 53 ECM proteins were detected in the hDNM, among which 35 proteins were also found in the pDNM. Other than these shared species of proteins, 33 were identified only in the pDNM and 18 specific proteins were found in the hDNM. These specific ECM proteins are listed in **Table 2**. Detailed matrisome analysis further revealed that the matrisome-associated proteins, which included the ECM-related proteins, the ECM regulators, and many secreted factors, were particularly enriched in the pDNM. Contrarily, the hDNM possessed a larger proportion of core matrisome proteins, including the ECM glycoproteins and proteoglycans (**Figure 3B** and **C**). The heatmap results showed that the relative abundance of the 35 shared proteins identified in the pDNM was 24, which was higher than that in the hDNM (11, **Figure 3D**). Additionally, the volcano plot shows that the number of up-regulated matrisome proteins in the pDNM was twice as many as that of the down-regulated

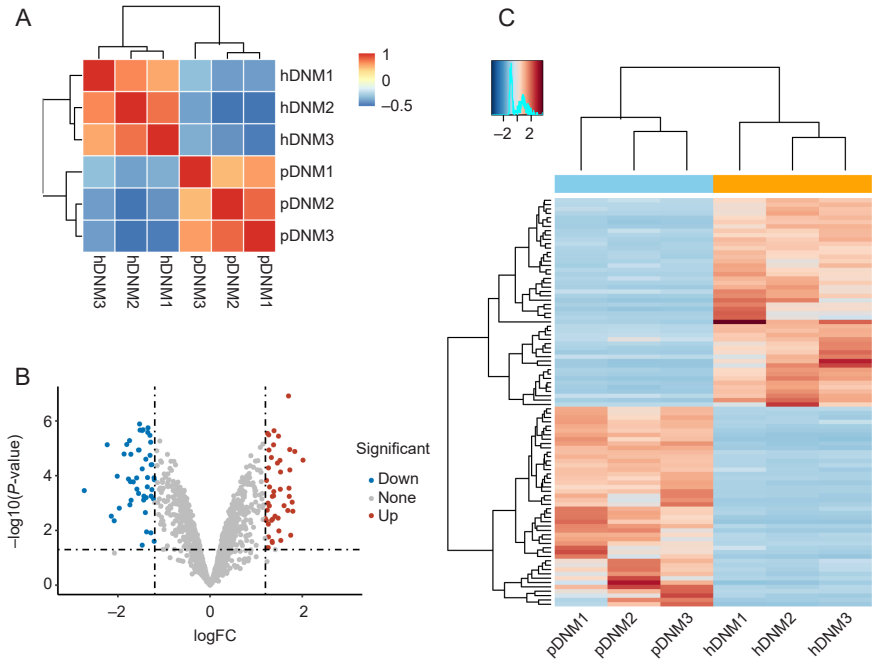


**Figure 2.** Proteomic analysis of hDNM and pDNM. (A) Unsupervised hierarchical clustering between the hDNM and pDNM using Pearson's correlation. (B) Volcano plot showing the differentially-expressed proteins between the hDNM and pDNM. (C) Heatmap and cluster dendrogram of protein abundances in the hDNM and pDNM. FC: fold change; hDNM: human decellularised nerve matrix; pDNM: porcine decellularised nerve matrix.

**Table 2. Specific dECM proteins identified only in the pDNM or hDNM**

| Classification | | pDNM | hDNM |
|---|---|---|---|
| Core matrisome | ECM glycoproteins | LAMB3, MXRA5, EDIL3, SLIT1, VWA3A, EMILIN3 | EMILIN2, CTGF, LAMA1, SRPX |
| | Collagens | None | COL6A6 |
| | Proteoglycans | None | None |
| ECM-associated proteins | ECM-related proteins | ELFN2, FREM2, C1QL4, PLXNA2, PLXNA4, ANXA9 | GPC5, FCN1, PLXNA3 |
| | ECM regulators | ADAMTS14, TIMP3, CTSG, MMP12, MEP1A, ADAMTS7, ADAMTS5 | FAM20C, ADAMTS21, ADAMTS15, ADAMTSL3 |
| | Secreted factors | WNT3A, BMP3, INHBA, MSTN, S100A4, NFSF15, FGF14, S100A13, ANGPTL7, HHIP, BRINP2, GDF3, FGF9 | MEGF11, IL4, GDF5, INHBB |

Note: dECM: decellularised extracellular matrix; ECM: extracellular matrix; hDNM: human decellularised nerve matrix; pDNM: porcine decellularised nerve matrix.

proteins (**Figure 3E**), among which the upregulated proteins were positively regulated with cellular proliferation (i.e., CSPG4, FGF2), migration (i.e., SLIT3, CSPG4, LAMA2), and maturation (i.e., FGF2). Among the three downregulated proteins, PODN negatively regulated cell proliferation and migration (**Figure 3E**). It is acknowledged that these diverse proteomic compositions found in dECMs can have strong regulatory effects on cell behaviour.

### Cellular behaviour regulated by hDNM and pDNM hydrogels

To easily examine the functionalities of both pDNM and hDNM for cell culture and regulating cellular behaviours *in vitro*, both dECM scaffolds were first converted into their corresponding hydrogels, i.e. pDNM-gel and hDNM-gel, respectively. Then, these hydrogels were employed to culture HSCs, a classic glial cell extracted from the human spinal nerve that can provide a simple, well-defined, and accessible mammalian *in vitro* model for investigating nerve cell and material interaction.[41] Cell viability, proliferation, migration, and functional expressions were systematically investigated and compared using hDNM-gel and pDNM-gel.

First, the cytocompatibility of both dECM hydrogels was assessed by live/dead staining. It should be emphasised that very few dead cells were identified after 48 hours of culture, indicating that both pDNM-gel and hDNM-gel were highly compatible with the HSCs (**Figure 4A**). Furthermore, it was also noticed that the total number of HSCs growing on both hDNM-gel and pDNM-gel were nearly double that of the control group, which suggested that the dECM hydrogels

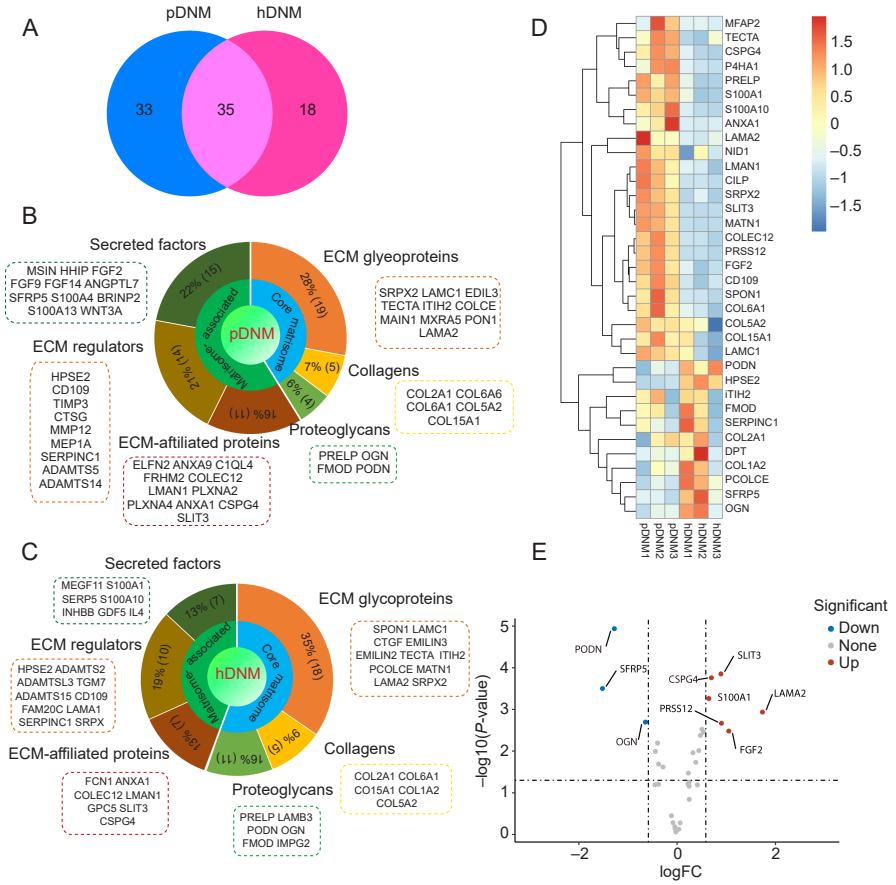


**Figure 3.** Matrisome analysis of the proteomic composition in pDNM and hDNM. (A) Venn diagram showing the number of ECM proteins detected in hDNM and pDNM. (B, C) Percentages of the ECM proteins and their corresponding matrisome subcategories identified in pDNM (B) and hDNM (C). (D) Heatmap representing significant distinctions in the co-expressed ECM proteins between pDNM and hDNM. The relative abundance of the 35 shared proteins identified in pDNM was higher than that in hDNM. (E) Volcano plot of the differentially expressed ECM proteins in pDNM compared to hDNM. The red and blue dots indicate the significantly up- and down-regulated ECM proteins, respectively ($n = 3$ for both pDNM and hDNM). ECM: extracellular matrix, hDNM: human decellularised nerve matrix; pDNM: porcine decellularised nerve matrix.

also promoted HSC proliferation. This was confirmed by immunofluorescence staining, when the cultured HSCs were double stained by EdU and S100 to label proliferating cells and Schwann cells, respectively. It was noted that the number of EdU/S100 co-expressing cells cultured on hDNM-gel and pDNM-gel were both significantly greater compared with the control group (**Figure 4B**). However, no significant difference was evident between the two hydrogel groups (**Figure 4C**). These results indicated that both hydrogels exhibited similar biological functions in facilitating HSC proliferation. Additionally, the migration of HSCs was evaluated using a wound healing assay. It was obvious that the HSCs migration was significantly facilitated on both the hDNM-gel and pDNM-gel within 24 hours, resulting in much higher migration rates, but there was not much difference between the two dECM hydrogel groups (**Figure 4D** and **E**).

Furthermore, to validate the bioactivities of the dECMs in promoting cell behaviours and for comparison, the mRNA levels of several genes, which are highly related to neuronal growth, remyelination, and differentiation, were assessed by qPCR. The results showed that both DNM hydrogels effectively upregulated the mRNA expression levels of MAP-2, GAP43, MBP, and MPZ, but no significant changes were evident regarding GFAP and S100β gene expression (**Figure 4F**). These results suggested that the dECM hydrogels contributed to facilitating HSC growth and remyelination but had a minor modulatory effect on their differentiation. Comparisons between the hDNM-gel and pDNM-gel groups revealed no significant discrepancies in the expression levels of the above-mentioned genes. The results from cell culture demonstrated that both hDNM and pDNM hydrogels exhibited similar bioactivities in regulating the survival, proliferation, migration, and maturation of cultured HSCs.

### α-Gal antigen and other immunogenic contents retained in hDNM and pDNM

Tissue-derived dECM materials, especially xenogeneic pDNM, inevitably contain small amounts of antigens and other biomolecules that might evoke host rejection and foreign body responses, and such molecules include α-Gal, MHC-1, and endotoxins.[42] To confirm the existence of these immunogens in hDNM and pDNM, we first evaluated the α-Gal antigen

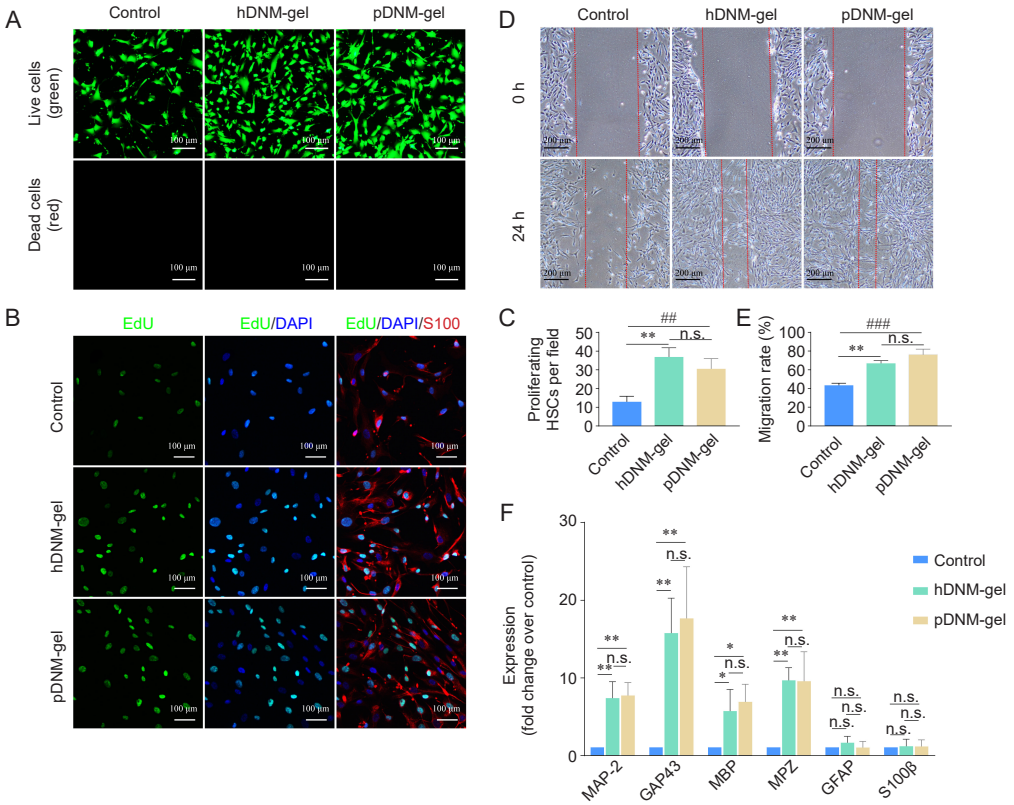


**Figure 4.** Bioactivities of both hDNM-gel and pDNM-gel in regulating the behaviours of cultured HSCs. (A) Representative fluorescence micrographs of the cultured HSCs on hDNM-gel and pDNM-gel after 48 hours of incubation and live/dead staining, compared to the control (no hydrogel). Scale bars: 100 μm. (B) Representative fluorescence confocal micrographs of HSCs cultured for 48 hours and immunostained with EdU (green), S100 (red), and DAPI (blue). Scale bars: 100 μm. (C) Number of proliferating ($EdU^+/S100^+$) HSCs in B. (D) Wound healing characterisation showing the wound gaps at 0 and 24 hours in the control, hDNM-gel, and pDNM-gel groups. Scale bars: 100 μm. (E) HSC migration based on the wound healing experiments in D ($n$ = 3). (F) MAP-2, GAP43, MBP, MPZ, GFAP, and S100β mRNA expression of the HSCs cultured on hDNM-gel and pDNM-gel were significantly upregulated compared to the control group ($n$ = 5). β-actin was used as the reference. Data are shown as the mean ± SD. $^*P < 0.05$, $^{**}P < 0.01$, $^{***}P < 0.001$. DAPI: 6-diamidino-2-phenylindole-dihydrochloride; dECM: decellularised extracellular matrix; EdU: 5-ethynyl-2′-deoxyuridine; GAP43: growth-associated protein 43; GFAP: glial fibrillary acidic protein; hDNM-gel: human decellularised nerve matrix hydrogel; HSCs: human Schwann cells; MAP-2: microtubule-associated protein-2; MBP: myelin basic protein; MPZ: myelin protein zero; n.s, not significant; pDNM-gel: porcine decellularised nerve matrix hydrogel.

that is commonly identified in non-primate mammalian tissues as a factor that may elicit severe immune rejection after implantation. The western blot results showed that no α-Gal was detectable in the hDNM, meanwhile, a large amount of α-Gal content was evident in the pDNM, which confirms that this antigen is a sort of specific protein that does not exist in human tissue. Once the pDNM was enzymatically hydrolysed by α-galactosidase, the α-Gal content was found to be effectively removed from the resulting pDNM-enzymolysis (**Figure 5A** and **B**). The immunofluorescence staining results using α-Gal antibody confirmed the absence of α-Gal in hDNM, and the presence of the Gal epitope in the pDNM was highly diminished once treated with α-Gal (**Figure 5C** and **D**). Furthermore, it was noticed that the abundant α-Gal antigen in raw porcine nerve tissues was significantly reduced after decellularisation (i.e., in pDNM), and further erased after hydrolysation (**Figure 5E**). These results suggested that although some α-Gal was present in the pDNM, the amount of this xenoantigen can be efficiently reduced by post-decellularisation modification.

Considering other possible factors that may lead to host rejection, another antigen, MHC-1, that may elicit host rejection was also assessed by western blotting. It was noted that MHC-1 was present in both hDNM and pDNM; however, the pDNM contained more MHC-1 antigen compared to the hDNM ($P < 0.01$; **Figure 5F** and **G**). Furthermore, we also evaluated endotoxin contamination in both dECMs using a kinetic turbidimetric technique, which revealed that hDNM and pDNM had similar contents of endotoxin (**Figure 5H**).

### Host immune responses to hDNM and pDNM in a humanised mouse model

To better assess the human immune response after implantation of DNMs, a humanised mouse model was established using the PBMC-NPG mice. These Hu-mice possess human

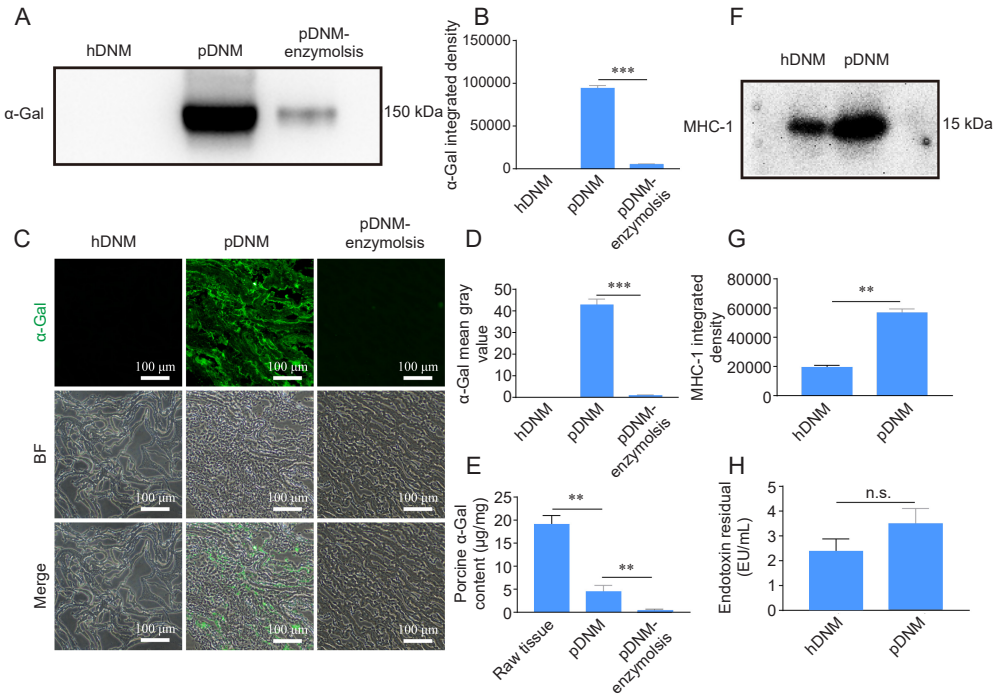


**Figure 5.** Detection of the immunogenic contents (α-Gal, MHC-1, and endotoxin) in hDNM and pDNM. (A, B) Western blot results and quantification of α-Gal antigen in hDNM, pDNM, and pDNM pre-treated with α-galactosidase (pDNM-enzymolysis). (C) Immunofluorescence staining and BF micrographs showing the presence of α-Gal antigen (green) within the hDNM, pDNM, and pDNM-enzymolysis samples. Scale bars: 100 μm. (D) Quantification of the immunoreactivity of α-Gal antigens. (E) Quantification of α-Gal content in raw porcine nerve tissues, pDNM, and pDNM after α-Gal treatment. (F) Western blot image and (G) quantification of the MHC-1 content in hDNM and pDNM. (H) Quantification of the endotoxin content in hDNM and pDNM. Data are presented as mean ± SD ($n = 3$). $^{**}P < 0.01$, $^{***}P < 0.001$. α-Gal: α-galactosidase; BF: bright field; hDNM: human decellularised nerve matrix; MHC-1: major histocompatibility complex 1; n.s.: not significant; pDNM: porcine decellularised nerve matrix.

immune cells that can respond to immunogens, including T- and B-cells.[43] The prepared hDNM, pDNM, and pDNM-enzymolysis were subcutaneously injected into the back of the Hu-mice. One week after injection, the subcutaneous tissue around the injection site of each Hu-mouse was sectioned for histological analysis, and the foreign body reactions were evaluated by the extent of cellular infiltration (**Figure 6A**). Unlike normal subcutaneous tissue in a humanised mouse model (control group), after administration of the dECM materials, larger cavities were observed, and cells could be seen to have intensively infiltrated into the injected area. The cell infiltration was particularly significant in the pDNM injected region, rather than the hDNM and pDNM-enzymolysis groups. It was interesting that the number of infiltrated cells in the pDNM-enzymolysis group was about the same as that of the hDNM group, suggesting similar foreign body responses post-implantation (**Figure 6B**).

To evaluate the adaptive immune responses of the implanted Hu-mice, 10 mg/mL hDNM, pDNM and pDNM-enzymolysis solutions were administered to PBMC-NPG mice through intravenous injection. One week after treatment, their venous blood was collected to identify and quantify the human leukocytes ($hCD45^+$) and their subpopulations, including B cells ($hCD45^+hCD19^+$), T helper cells ($hCD3^+hCD4^+$), and cytotoxic T cells ($hCD3^+hCD8^+$) using flow cytometry. First, it was noted that the percentage of human immune cells in the blood was detectable in the control group (3.20 ± 0.25%), although the mouse leukocytes ($mCD45^+$) were still responsible for the dominant percentage (80.35 ± 3.47%; **Figure 6C** and **D**). Meanwhile, all the dECM-injected Hu-mice exhibited a significantly increased number of human immune cells. The administration of pDNM led to the greatest number of leukocytes ($hCD45^+$ 17.96 ± 1.17%). The hDNM-treated group resulted in a slightly better immune response but the percentage of $hCD45^+$ cells still increased to 11.06 ± 0.96%. Surprisingly, the introduction of pDNM-enzymolysis elicited minimal host immune response, with the fraction of $hCD45^+$ cells only elevated to 6.46 ± 1.16%, which was even less than that of the hDNM group. A similar trend was observed regarding the number of human B cells. The total number of B cells increased to 730 ± 48 per 1000 cells after pDNM administration, which was much greater than that of the hDNM injected Hu-mice (**Figure 6E**). Meanwhile, the injection of pDNM-enzymolysis induced a very small increment of the human B cell population, which was close to that of the Hu-mice without materials implantation.

We next explored the different T cell subtypes and their accumulation after injection of dECMs into the Hu-mice (**Figure 7A**), which can verify the type of host immune responses to the implantable biomaterials, whether they

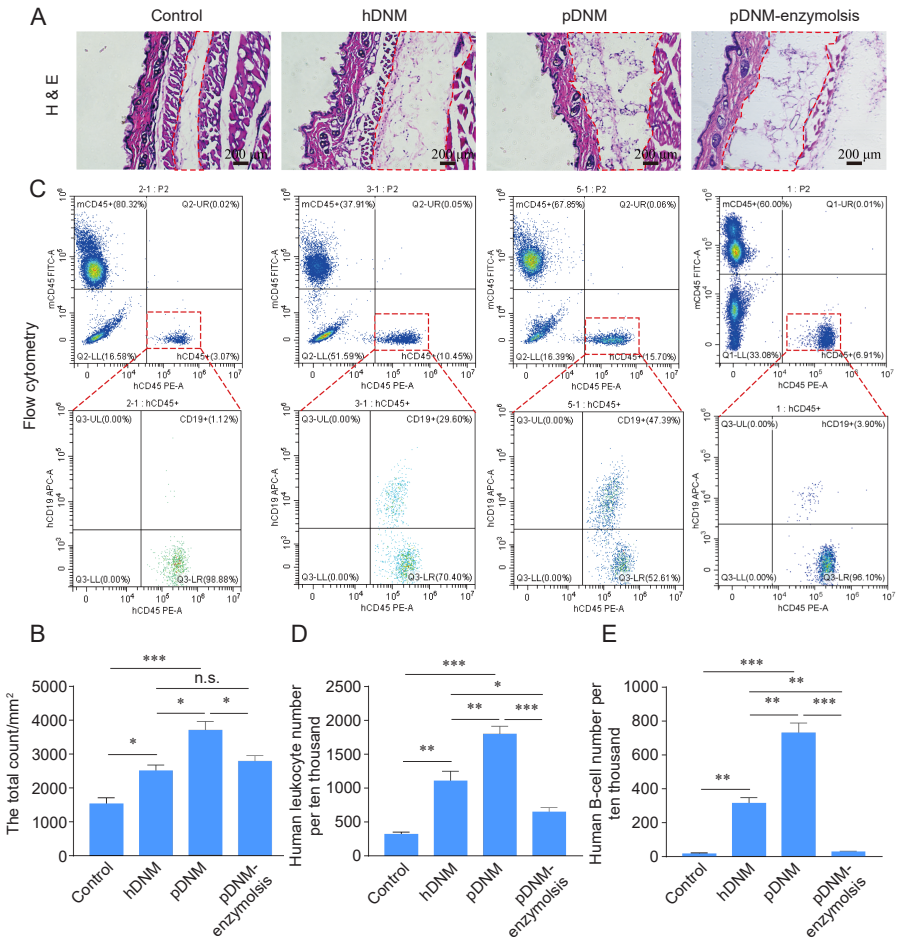


**Figure 6.** Host immune responses to subcutaneously injected hDNM, pDNM, and pDNM-enzymolysis in a humanised mouse model. Hu-mice received the same volume of sterile saline as the control. (A) H&E staining of the subcutaneous tissues sectioned from the Hu-mice in each group. Scale bars: 200 μm. (B) The total number of infiltrating cells in the dotted box in A based on H&E histological staining. (C) Flow cytometry results showing the human immune cells after treatment. (D, E) Quantitative analysis of the density of human leukocytes (hCD45$^+$) (D) and the density of human B cells (hCD45$^+$ hCD19$^+$) (E) based on flow cytometric assessments. Data are presented as mean ± SD ($n$ = 3). *$P$ < 0.05, **$P$ < 0.01, ***$P$ < 0.001. H&E: haematoxylin-eosin; hDNM: human decellularised nerve matrix; n.s: not significant; pDNM: porcine decellularised nerve matrix.

are pro-remodelling or pro-inflammatory. It was noted that the introduction of pDNM led to the greatest number of T cells. Though the allogeneic hDNM also resulted in a larger T cell repopulation, this was still much less than that of pDNM group. The hydrolysed pDNM (pDNM-enzymolysis), however, manifested a much slower T cell repopulation; the density of T cells was even smaller than that of the hDNM group (**Figure 7B**). Such distinct differences between the hDNM, pDNM, and pDNM-enzymolysis groups were further confirmed by sorting the T cells into two subtypes, T helper cells and cytotoxic T cells. Both the hDNM- and pDNM-enzymolysis-injected mice were proven to have more T helper cells and far fewer cytotoxic T cells compared to those of the pDNM group (**Figure 7C** and **D**), which resulted in a higher T helper cells/cytotoxic T cells ratio, implicating a pro-remodelling phenotype. Interestingly, the pDNM-enzymolysis group exhibited similar host responses to the hDNM group in terms of human adaptive immune responses.

## Discussion

Porcine-derived dECM biomaterials are potentially useful for repair and reconstruction of xenogenic tissues in the field of tissue engineering and regenerative medicine.[44, 45] Given the similarity in gene sequences between humans and pigs,[46] porcine tissue-derived materials are currently viewed as attractive alternatives in regenerative medicine. Previously, we have successfully prepared dECM scaffolds and their derivative hydrogel from porcine sciatic nerve tissue, namely pDNM and pDNM-gel, by following rather straightforward decellularisation and digestion protocols, and their bioactivity and processibility have been proven in terms of promoting peripheral nerve regeneration and functional recovery *in vitro* and *in vivo*.[17-22] To verify that such mammal-derived xenografts can be used as an appropriate substitute for future clinical applications, herein, a comparative study concerning the variations between the allogeneic hDNM and xenogeneic pDNM was systematically implemented. Unlike our previous reports, this study focuses on comparisons between the

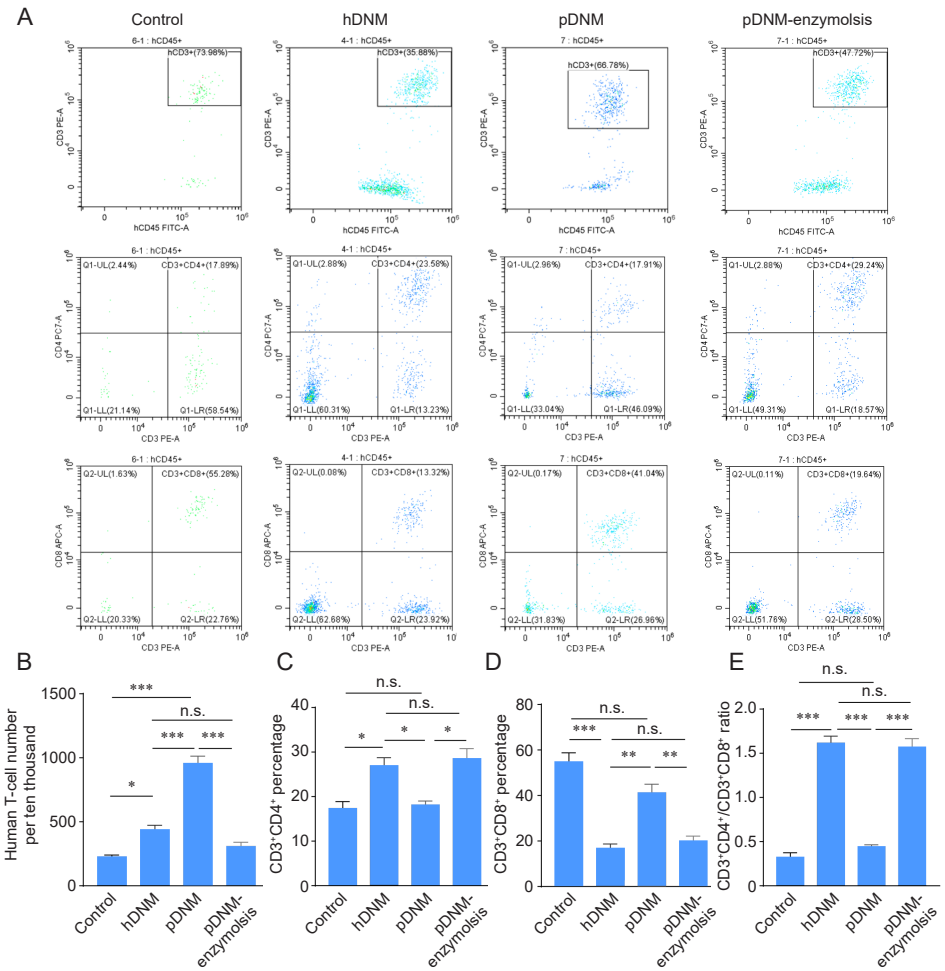


**Figure 7.** Evaluation of T cell repopulation and their subtypes after injection of hDNM, pDNM, or pDNM-enzymolysis into humanised mice, analysed using flow cytometry. (A) T cells ($hCD45^+hCD3^+$) and their subtypes, including T helper cells ($hCD3^+hCD4^+$) and cytotoxic T cells ($hCD3^+hCD8^+$). (B) The density of total human T cells after introducing the dECMs into Hu-mice. (C) The percentage of the T helper cells ($hCD3^+hCD4^+$). (D) The percentage of cytotoxic T cells ($hCD3^+hCD8^+$). (E) The ratios of T helper cells/cytotoxic T cells. The data are expressed as mean ± SD ($n = 3$). $^*P < 0.05$, $^{**}P < 0.01$, $^{***}P < 0.001$ . hDNM: human decellularised nerve matrix; n.s: not significant; pDNM: porcine decellularised nerve matrix.

microstructures of the scaffolds, proteomic compositions, biological functions of the dECM hydrogels, and more importantly, the immunogenicity for potential implantation into human bodies. Furthermore, a consecutive question that we managed to answer is, if pDNM might result in severe host rejection following clinical implantation, can it be modified to produce a more clinically-satisfactory outcome?

We first characterised the microscopic ultrastructures of both hDNM and pDNM scaffolds using SEM. Both decellularised matrices retained the structures of the nerve fascicles and interfascicular connective tissues, which are consistent with the high-resolution topography of the native peripheral nerve fascicles reported by Yan et al.[47] These longitudinally-aligned microtubes function in guiding axonal growth.[22]

It has been shown that the diverse proteomic compositions of dECMs play a vital role in regulating cellular phenotypes and behaviours.[48, 49] Therefore, we systematically compared the compositions of hDNM and pDNM through proteomic analysis regarding all the protein species and specifically the ECM matrisome. We first realised that most of the constituent biomolecules shared similar contents and functionalities between hDNM and pDNM. However, it was also noticed that pDNM possessed a slightly greater number and higher abundance of matrisome proteins compared to hDNM. Especially, some ECM proteins (such as CSPG4, FGF2, SLIT3, and LAMA2) were only identified in pDNM, which can positively facilitate cellular proliferation, migration, differentiation, and maturation. Meanwhile the core matrisome PODN, which may negatively regulate the above-mentioned biological processes, was far less abundant than that identified in the hDNM. We speculate that the similarity of the proteomic compositions of both hDNM and pDNM assure the fundamental functionalities of the tissue-specific dECM materials, but that the abundant ECM components found in the pDNM may provide higher bioactivities in facilitating nerve regeneration and functionalisation.

Therefore, to validate and compare the bioactivities of the dECM materials, primary HSCs were cultured on dECM hydrogels prepared from hDNM and pDNM. Since the cells cultured on dECM scaffold are typically hard to be visualised, hydrogel-based dECM materials were employed rather than the scaffolds themselves. Although some biomacromolecules in the DNM might undergo degradation or denaturation during enzymatic digestion, most of the dECM proteins were retained in the obtained hydrogels.[50, 51] Throughout all the *in vitro* characterisations, it has been acknowledged that both the hDNM and pDNM hydrogels exhibited similar functionalities in promoting HSC proliferation, migration, and specific gene expressions. This result seems be inconsistent with our normal logic. We speculate the reason may be attributed to degradation of some components when both dECMs are digested into hydrogel. Thus, further, we should characterise the composition of hDNM-gel and pDNM-gel using quantitative proteomic analysis.

Finally, the potential immunological responses in the human body are key to the viability of the various xenografts in clinical application, for example, porcine-derived dECM materials. In this study, we first evaluated the non-primate antigens and some other immunogenic components in the DNMs to assess potential adverse host responses. Among these detected immunogens, the α-Gal component was only evident in the pDNM, as we expected. In fact, it was not only present in the pDNM but also in considerable amounts that might evoke severe immune responses or host rejection in the human body. For this reason, we managed to remove the α-Gal content from the pDNM through enzymatic hydrolysation. It was realised that the α-Gal antigen could be effectively diminished using α-Gal.

Since there are serious ethical issues and difficulties related to experiments on real human bodies, we established a humanised mouse model to simulate the human immune responses to the administration of both hDNM and pDNM, and additionally, the α-Gal-eliminated pDNM (termed pDNM-enzymolysis) *in vivo*. Histological characterisation of the material-injected subcutaneous tissues showed that the introduction of pDNM evoked much more significant cell infiltration compared to that of the hDNM group. Furthermore, studies on the human immune cells in the Hu-mice showed that all the injected DNM materials stimulated considerable immunoreactions and resulted in significant proliferation of immune cells, including B cells and T cells. Obviously, the adaptive immune responses in the pDNM-injected Hu-mice were much more severe than those of the hDNM or pDNM-enzymolysis groups. Further evaluation of the T cell subpopulations revealed that the introduction of pDNM induced fewer T helper cells ($hCD3^+hCD4^+$) and more cytotoxic T-cells ($hCD3^+hCD8^+$), compared to the hDNM. These results suggested that the allogeneic hDNM stimulated a pro-remodelling response, whereas the xenogeneic pDNM intended to elicit a more pro-inflammatory immune reaction.

Since the α-Gal epitope usually serves as the key factor that evokes severe human immune responses, we conjectured that the removal of the α-Gal antigen might alleviate the hostile host responses against the porcine-derived xenografts. To this end, the pDNM-enzymolysis was also tested in the Hu-mice model. The adverse immune responses were found to be highly diminished upon removing the α-Gal content from the pDNM, which was comparable to or even better than that of the hDNM group. In the meantime, the T cells in the pDNM-enzymolysis Hu-mice dominantly retained the pro-regenerative phenotype that may further contribute to tissue regeneration, which was similar to those of the hDNM group. Consequently, considering the translational potential of the xenogeneic pDNM, we believe that this sort of porcine-derived dECM material can be beneficial for future clinical applications, once its residual α-Gal antigen has been removed. The α-Gal content can be properly eliminated by enzymatic hydrolysation, otherwise, the source tissues should be obtained from α-Gal gene-knockout pigs. Currently, the α-Gal epitope-induced immune response has drawn increasing attention for development of implantable dECM biomaterials which may be critical to their clinical translation. However, in the present study, we have not evaluated the potential transmission risk of porcine endogenous retroviruses. They are γ-retroviruses integrated in the genome of all pigs and can be transmitted from pig to human cells, leading to immunodeficiencies and tumors.[52, 53] Further work will be needed to either detect the presence of porcine endogenous retroviruses in pDNM using qPCR methods or directly harvest nerves from genetically-modified pigs.

In this study, two dECM materials derived from human and porcine nerve tissues (hDNM and pDNM) were prepared and compared in terms of their microstructures, compositions, biological performance, and immunogenicity. Basically, both hDNM and pDNM shared almost the same ultrastructure and comparable proteomic compositions. The hydrogels derived from both hDNM and pDNM also resulted in similar regulation of HSC behaviours. Distinct differences were evident regarding the specific antigens and their induced human host immune responses. pDNM contains a few xenoantigens, including α-Gal and MHC-1, that evoked more adverse host responses in a humanised mouse model, compared to the hDNM. After removing most of the α-Gal content using α-Gal hydrolysation, the human host responses were alleviated and became pro-regenerative. It was realized that pDNM-enzymolysis performed similarly to the hDNM and induced similar immune responses. This experimental evidence suggests that the removal of α-Gal antigen is key to the future application of pDNM and pDNM-derived biomaterials. Furthermore, the current study may provide a springboard for both xenogeneic dECM studies and harnessing such functional biomaterials for use at the bedside.

**Author contributions**

Methodology, material preparation, data collection: RL, WY, and ZR; *in vivo* test support, statistical analysis: RL and SQ; conceptualisation and design: YY, QZ, and XL; funding acquisition, supervision, manuscript finalisation, and project administration: YB; study conceptualisation and design, supervision, data interpretation, project administration, funding acquisition, manuscript drafting and refining: DQ. All authors approved the final version of this manuscript.

**Financial support**

This study was supported by the National Natural Science Foundation of China (Nos. 51903255 and 52073314), The Key Areas Research and Development Program of Guangdong Province (No. 2020B1111150003), and Science and Technology Program of Guangzhou City (No. 201904010364).

**Acknowledgement**

The authors would like to thank Ms. Weizhen Tang (a laboratory assistant in Guangdong Engineering Technology Research Centre for Functional Biomaterials, School of Materials Science and Engineering, Sun Yat-sen University) for her assistance in cell culture experiments.

**Conflicts of interest statement**

The authors declare that they have no competing financial interests or personal relationships that could have appeared to influence the work reported in this study. No conflicts of interest exist between Guangzhou Zhongda Medical Equipment Co., Ltd. and the publication of this paper.

Editor note: Daping Quang are an Editorial Board member of *Biomaterials Translational*. She is blinded from reviewing or making decisions on the manuscript. The article was subject to the journal's standard procedures, with peer review handled independently of this Editorial Board member and her research group.



**Additional files**

***Additional Figure 1:*** A flow chart of the *in vivo* study.

***Additional Figure 2:*** Scanning electron micrographs showing cross-sectional views of a native human nerve and a native porcine nerve.

1. Krishtul, S.; Baruch, L.; Machluf, M. Processed tissue–derived extracellular matrices: tailored platforms empowering diverse therapeutic applications. *Adv Funct Mater.* **2020**, *30*, 1900386.
2. Garreta, E.; Oria, R.; Tarantino, C.; Pla-Roca, M.; Prado, P.; Fernández-Avilés, F.; Campistol, J. M.; Samitier, J.; Montserrat, N. Tissue engineering by decellularization and 3D bioprinting. *Mater Today.* **2017**, *20*, 166-178.
3. Hussey, G. S.; Dziki, J. L.; Badylak, S. F. Extracellular matrix-based materials for regenerative medicine. *Nat Rev Mater.* 2018, *3*, 159-173.
4. Li, T.; Javed, R.; Ao, Q. Xenogeneic decellularized extracellular matrix-based biomaterials for peripheral nerve repair and regeneration. *Curr Neuropharmacol.* **2021**, *19*, 2152-2163.
5. Zouhair, S.; Sasso, E. D.; Tuladhar, S. R.; Fidalgo, C.; Vedovelli, L.; Filippi, A.; Borile, G.; Bagno, A.; Marchesan, M.; Giorgio, R.; Gregori, D.; Wolkers, W. F.; Romanato, F.; Korossis, S.; Gerosa, G.; Iop, L. A comprehensive comparison of bovine and porcine decellularized pericardia: new insights for surgical applications. *Biomolecules.* **2020**, *10*, 371.
6. Capella-Monsonís, H.; De Pieri, A.; Peixoto, R.; Korntner, S.; Zeugolis, D. I. Extracellular matrix-based biomaterials as adipose-derived stem cell delivery vehicles in wound healing: a comparative study between a collagen scaffold and two xenografts. *Stem Cell Res Ther.* **2020**, *11*, 510.
7. Bowers, S. L.; Banerjee, I.; Baudino, T. A. The extracellular matrix: at the center of it all. *J Mol Cell Cardiol.* **2010**, *48*, 474-482.
8. Keane, T. J.; Londono, R.; Turner, N. J.; Badylak, S. F. Consequences of ineffective decellularization of biologic scaffolds on the host response. *Biomaterials.* **2012**, *33*, 1771-1781.
9. Badylak, S. F. Xenogeneic extracellular matrix as a scaffold for tissue reconstruction. *Transpl Immunol.* **2004**, *12*, 367-377.
10. Badylak, S. F.; Gilbert, T. W. Immune response to biologic scaffold materials. *Semin Immunol.* **2008**, *20*, 109-116.
11. Kasper, M.; Deister, C.; Beck, F.; Schmidt, C. E. Bench-to-bedside lessons learned: commercialization of an acellular nerve graft. *Adv Healthc Mater.* **2020**, *9*, e2000174.
12. Yang, L. M.; Liu, X. L.; Zhu, Q. T.; Zhang, Y.; Xi, T. F.; Hu, J.; He, C. F.; Jiang, L. Human peripheral nerve-derived scaffold for tissue-engineered nerve grafts: histology and biocompatibility analysis. *J Biomed Mater Res B Appl Biomater.* **2011**, *96*, 25-33.
13. Colwell, A. S.; Longaker, M. T.; Lorenz, H. P. Mammalian fetal organ regeneration. *Adv Biochem Eng Biotechnol.* **2005**, *93*, 83-100.
14. Sicari, B. M.; Johnson, S. A.; Siu, B. F.; Crapo, P. M.; Daly, K. A.; Jiang, H.; Medberry, C. J.; Tottey, S.; Turner, N. J.; Badylak, S. F. The effect of source animal age upon the in vivo remodeling characteristics of an extracellular matrix scaffold. *Biomaterials.* **2012**, *33*, 5524-5533.
15. Badylak, S. F. The extracellular matrix as a biologic scaffold material. *Biomaterials.* **2007**, *28*, 3587-3593.
16. Seif-Naraghi, S. B.; Singelyn, J. M.; Salvatore, M. A.; Osborn, K. G.; Wang, J. J.; Sampat, U.; Kwan, O. L.; Strachan, G. M.; Wong, J.; Schup-Magoffin, P. J.; Braden, R. L.; Bartels, K.; DeQuach, J. A.; Preul, M.; Kinsey, A. M.; DeMaria, A. N.; Dib, N.; Christman, K. L. Safety and efficacy of an injectable extracellular matrix hydrogel for treating myocardial infarction. *Sci Transl Med.* **2013**, *5*, 173ra125.
17. Chen, S.; Du, Z.; Zou, J.; Qiu, S.; Rao, Z.; Liu, S.; Sun, X.; Xu, Y.; Zhu, Q.; Liu, X.; Mao, H. Q.; Bai, Y.; Quan, D. Promoting neurite growth and schwann cell migration by the harnessing decellularized nerve matrix onto nanofibrous guidance. *ACS Appl Mater Interfaces.* **2019**, *11*, 17167-17176.
18. Zheng, C.; Yang, Z.; Chen, S.; Zhang, F.; Rao, Z.; Zhao, C.; Quan, D.; Bai, Y.; Shen, J. Nanofibrous nerve guidance conduits decorated with decellularized matrix hydrogel facilitate peripheral nerve injury repair. *Theranostics.* **2021**, *11*, 2917-2931.
19. Deng, R.; Luo, Z.; Rao, Z.; Lin, Z.; Chen, S.; Zhou, J.; Zhu, Q.; Liu, X.; Bai, Y.; Quan, D. Decellularized extracellular matrix containing electrospun fibers for nerve regeneration: a comparison between core–shell structured and preblended composites. *Adv Fiber Mater.* **2022**, *4*, 503-519.
20. Xu, Y.; Zhou, J.; Liu, C.; Zhang, S.; Gao, F.; Guo, W.; Sun, X.; Zhang, C.; Li, H.; Rao, Z.; Qiu, S.; Zhu, Q.; Liu, X.; Guo, X.; Shao, Z.; Bai, Y.; Zhang, X.; Quan, D. Understanding the role of tissue-specific decellularized spinal cord matrix hydrogel for neural stem/progenitor cell microenvironment reconstruction and spinal cord injury. *Biomaterials.* **2021**, *268*, 120596.
21. Lin, T.; Liu, S.; Chen, S.; Qiu, S.; Rao, Z.; Liu, J.; Zhu, S.; Yan, L.; Mao, H.; Zhu, Q.; Quan, D.; Liu, X. Hydrogel derived from porcine decellularized nerve tissue as a promising biomaterial for repairing peripheral nerve defects. *Acta Biomater.* **2018**, *73*, 326-338.
22. Rao, Z.; Lin, T.; Qiu, S.; Zhou, J.; Liu, S.; Chen, S.; Wang, T.; Liu, X.; Zhu, Q.; Bai, Y.; Quan, D. Decellularized nerve matrix hydrogel scaffolds with longitudinally oriented and size-tunable microchannels for peripheral nerve regeneration. *Mater Sci Eng C Mater Biol Appl.* **2021**, *120*, 111791.
23. Keane, T. J.; Badylak, S. F. The host response to allogeneic and xenogeneic biological scaffold materials. *J Tissue Eng Regen Med.* **2015**, *9*, 504-511.
24. Brown, B. N.; Londono, R.; Tottey, S.; Zhang, L.; Kukla, K. A.; Wolf, M. T.; Daly, K. A.; Reing, J. E.; Badylak, S. F. Macrophage phenotype as a predictor of constructive remodeling following the implantation of biologically derived surgical mesh materials. *Acta Biomater.* **2012**, *8*, 978-987.

25. Brown, B. N.; Valentin, J. E.; Stewart-Akers, A. M.; McCabe, G. P.; Badylak, S. F. Macrophage phenotype and remodeling outcomes in response to biologic scaffolds with and without a cellular component. *Biomaterials.* **2009**, *30*, 1482-1491.
26. Galili, U. Interaction of the natural anti-Gal antibody with alpha-galactosyl epitopes: a major obstacle for xenotransplantation in humans. *Immunol Today.* **1993**, *14*, 480-482.
27. Mestas, J.; Hughes, C. C. Of mice and not men: differences between mouse and human immunology. *J Immunol.* **2004**, *172*, 2731-2738.
28. Qiu, S.; Rao, Z.; He, F.; Wang, T.; Xu, Y.; Du, Z.; Yao, Z.; Lin, T.; Yan, L.; Quan, D.; Zhu, Q.; Liu, X. Decellularized nerve matrix hydrogel and glial-derived neurotrophic factor modifications assisted nerve repair with decellularized nerve matrix scaffolds. *J Tissue Eng Regen Med.* **2020**, *14*, 931-943.
29. Devaud, Y. R.; Avilla-Royo, E.; Trachsel, C.; Grossmann, J.; Martin, I.; Lutolf, M. P.; Ehrbar, M. Label-free quantification proteomics for the identification of mesenchymal stromal cell matrisome inside 3D poly(ethylene glycol) hydrogels. *Adv Healthc Mater.* **2018**, *7*, e1800534.
30. UniProt Consortium. UniProt: the universal protein knowledgebase in 2021. *Nucleic Acids Res.* **2021**, *49*, D480-D489.
31. Morfeld, P. Controlling the false discovery rate in many SMR analyses. *J Occup Environ Med.* **2016**, *58*, e21-22.
32. Naba, A.; Clauser, K. R.; Ding, H.; Whittaker, C. A.; Carr, S. A.; Hynes, R. O. The extracellular matrix: Tools and insights for the "omics" era. *Matrix Biol.* **2016**, *49*, 10-24.
33. Schneider, C. A.; Rasband, W. S.; Eliceiri, K. W. NIH image to ImageJ: 25 years of image analysis. *Nat Methods.* **2012**, *9*, 671-675.
34. Bubner, B.; Baldwin, I. T. Use of real-time PCR for determining copy number and zygosity in transgenic plants. *Plant Cell Rep.* **2004**, *23*, 263-271.
35. Stone, K. R.; Ayala, G.; Goldstein, J.; Hurst, R.; Walgenbach, A.; Galili, U. Porcine cartilage transplants in the cynomolgus monkey. III. Transplantation of alpha-galactosidase-treated porcine cartilage. *Transplantation.* **1998**, *65*, 1577-1583.
36. Percie du Sert, N.; Hurst, V.; Ahluwalia, A.; Alam, S.; Avey, M. T.; Baker, M.; Browne, W. J.; Clark, A.; Cuthill, I. C.; Dirnagl, U.; Emerson, M.; Garner, P.; Holgate, S. T.; Howells, D. W.; Karp, N. A.; Lazic, S. E.; Lidster, K.; MacCallum, C. J.; Macleod, M.; Pearl, E. J.; Petersen, O. H.; Rawle, F.; Reynolds, P.; Rooney, K.; Sena, E. S.; Silberberg, S. D.; Steckler, T.; Würbel, H. The ARRIVE guidelines 2.0: Updated guidelines for reporting animal research. *PLoS Biol.* **2020**, *18*, e3000410.
37. Lan, P.; Tonomura, N.; Shimizu, A.; Wang, S.; Yang, Y. G. Reconstitution of a functional human immune system in immunodeficient mice through combined human fetal thymus/liver and CD34$^+$ cell transplantation. *Blood.* **2006**, *108*, 487-492.
38. Khan, S.; Kaihara, K. A. Single-cell RNA-sequencing of peripheral blood mononuclear cells with ddSEQ. *Methods Mol Biol.* **2019**, *1979*, 155-176.
39. Wang, R. M.; Johnson, T. D.; He, J.; Rong, Z.; Wong, M.; Nigam, V.; Behfar, A.; Xu, Y.; Christman, K. L. Humanized mouse model for assessing the human immune response to xenogeneic and allogeneic decellularized biomaterials. *Biomaterials.* **2017**, *129*, 98-110.
40. Crapo, P. M.; Medberry, C. J.; Reing, J. E.; Tottey, S.; van der Merwe, Y.; Jones, K. E.; Badylak, S. F. Biologic scaffolds composed of central nervous system extracellular matrix. *Biomaterials.* **2012**, *33*, 3539-3547.
41. Behan, B. L.; DeWitt, D. G.; Bogdanowicz, D. R.; Koppes, A. N.; Bale, S. S.; Thompson, D. M. Single-walled carbon nanotubes alter Schwann cell behavior differentially within 2D and 3D environments. *J Biomed Mater Res A.* **2011**, *96*, 46-57.
42. Aamodt, J. M.; Grainger, D. W. Extracellular matrix-based biomaterial scaffolds and the host response. *Biomaterials.* **2016**, *86*, 68-82.
43. Walsh, N. C.; Kenney, L. L.; Jangalwe, S.; Aryee, K. E.; Greiner, D. L.; Brehm, M. A.; Shultz, L. D. Humanized mouse models of clinical disease. *Annu Rev Pathol.* **2017**, *12*, 187-215.
44. Kočí, Z.; Výborný, K.; Dubišová, J.; Vacková, I.; Jäger, A.; Lunov, O.; Jiráková, K.; Kubinová, Š. Extracellular matrix hydrogel derived from human umbilical cord as a scaffold for neural tissue repair and its comparison with extracellular matrix from porcine tissues. *Tissue Eng Part C Methods.* **2017**, *23*, 333-345.
45. Tan, Q. W.; Zhang, Y.; Luo, J. C.; Zhang, D.; Xiong, B. J.; Yang, J. Q.; Xie, H. Q.; Lv, Q. Hydrogel derived from decellularized porcine adipose tissue as a promising biomaterial for soft tissue augmentation. *J Biomed Mater Res A.* **2017**, *105*, 1756-1764.
46. Bikhet, M.; Morsi, M.; Hara, H.; Rhodes, L. A.; Carlo, W. F.; Cleveland, D.; Cooper, D. K. C.; Iwase, H. The immune system in infants: Relevance to xenotransplantation. *Pediatr Transplant.* **2020**, *24*, e13795.
47. Yan, L.; Guo, Y.; Qi, J.; Zhu, Q.; Gu, L.; Zheng, C.; Lin, T.; Lu, Y.; Zeng, Z.; Yu, S.; Zhu, S.; Zhou, X.; Zhang, X.; Du, Y.; Yao, Z.; Lu, Y.; Liu, X. Iodine and freeze-drying enhanced high-resolution MicroCT imaging for reconstructing 3D intraneural topography of human peripheral nerve fascicles. *J Neurosci Methods.* **2017**, *287*, 58-67.
48. Spang, M. T.; Christman, K. L. Extracellular matrix hydrogel therapies: in vivo applications and development. *Acta Biomater.* **2018**, *68*, 1-14.
49. Bi, H.; Ye, K.; Jin, S. Proteomic analysis of decellularized pancreatic matrix identifies collagen V as a critical regulator for islet organogenesis from human pluripotent stem cells. *Biomaterials.* **2020**, *233*, 119673.
50. Choudhury, D.; Yee, M.; Sheng, Z. L. J.; Amirul, A.; Naing, M. W. Decellularization systems and devices: State-of-the-art. *Acta Biomater.* **2020**, *115*, 51-59.
51. Xing, H.; Lee, H.; Luo, L.; Kyriakides, T. R. Extracellular matrix-derived biomaterials in engineering cell function. *Biotechnol Adv.* **2020**, *42*, 107421.
52. Yue, Y.; Xu, W.; Kan, Y.; Zhao, H. Y.; Zhou, Y.; Song, X.; Wu, J.; Xiong, J.; Goswami, D.; Yang, M.; Lamriben, L.; Xu, M.; Zhang, Q.; Luo, Y.; Guo, J.; Mao, S.; Jiao, D.; Nguyen, T. D.; Li, Z.; Layer, J. V.; Li, M.; Paragas, V.; Youd, M. E.; Sun, Z.; Ding, Y.; Wang, W.; Dou, H.; Song, L.; Wang, X.; Le, L.; Fang, X.; George, H.; Anand, R.; Wang, S. Y.; Westlin, W. F.; Güell, M.; Markmann, J.; Qin, W.; Gao, Y.; Wei, H. J.; Church, G. M.; Yang, L. Extensive germline genome engineering in pigs. *Nat Biomed Eng.* **2021**, *5*, 134-143.
53. Niu, D.; Wei, H. J.; Lin, L.; George, H.; Wang, T.; Lee, I. H.; Zhao, H. Y.; Wang, Y.; Kan, Y.; Shrock, E.; Lesha, E.; Wang, G.; Luo, Y.; Qing, Y.; Jiao, D.; Zhao, H.; Zhou, X.; Wang, S.; Wei, H.; Güell, M.; Church, G. M.; Yang, L. Inactivation of porcine endogenous retrovirus in pigs using CRISPR-Cas9. *Science.* **2017**, *357*, 1303-1307.

Received: November 17, 2022
Revised: December 6, 2022
Accepted: March 8, 2023
Available online: September 28, 2023